A Spectroscopic Analysis of Blue and Ultraviolet Upconverted Emissions from $Gd_3Ga_5O_{12}:Tm^{3+}$, Yb^{3+} Nanocrystals

Fabiano Pandozzi,[†] Fiorenzo Vetrone,[†] John-Christopher Boyer,[†] Rafik Naccache,[†] John A. Capobianco,*[,†] Adolfo Speghini,[‡] and Marco Bettinelli[‡]

Department of Chemistry and Biochemistry, Concordia University, 7141 Sherbrooke Street West, Montreal, QC, H4B 1R6, Canada, and Dipartimento Scientifico e Tecnologico, Università di Verona, and INSTM, UdR Verona, Ca' Vignal, Strada Le Grazie 15, I-37134 Verona, Italy

Received: April 27, 2005; In Final Form: July 11, 2005

The spectroscopic behavior of gadolinium gallium garnet ($Gd_3Ga_5O_{12}$, GGG) nanocrystals codoped with 1% each of Tm^{3+} and Yb^{3+} prepared via a solution combustion synthesis procedure was investigated. Initial excitation of the codoped nanocrystals with 465.8 nm (into the $^1G_4$ state) showed a dominant blue-green emission ascribed to the $^1G_4-{}^3H_6$ transition as well as red and NIR emissions from the $^1G_4-{}^3F_4$ and $^1G_4-{}^3H_5/{}^3H_4-{}^3H_6$ transitions, respectively. Excitation at this wavelength (465.8 nm) showed the existence of a $Tm^{3+} \rightarrow Yb^{3+}$ energy transfer process evidenced by the presence of the $^2F_{5/2}-{}^2F_{7/2}$ Yb^{3+} emission in the NIR emission spectrum. The decay time constants proved that the transfer of energy occurred via the $^3H_4$ state. Following excitation of the Yb^{3+} ion with 980 nm, intense upconverted emission was observed. Emissions in the UV ($^1D_2-{}^3H_6$), blue ($^1D_2-{}^3F_4$), blue-green ($^1G_4-{}^3H_6$), red ($^1G_4-{}^3F_4$), and NIR ($^1G_4-{}^3H_5/{}^3H_4-{}^3H_6$) were observed and were the direct result of subsequent transfers of energy from the Yb^{3+} ion to the Tm^{3+} ion. Power dependence studies showed a deviation from expected values for the number of photons involved in the upconversion thus indicating a saturation of the upconversion process. An energy transfer efficiency of 0.576 was determined experimentally.

1. Introduction

Advances in inorganic crystal synthesis have led to the ability to produce nanocrystalline particles suitable for spectroscopic studies, which are characterized as having sizes generally below 100 nm. Synthesis techniques presented in the literature are wide ranging from the very complex to the very simple (examples include combustion synthesis, sol−gel synthesis, wet chemical synthesis, etc.). These preparation methods capable of producing luminescent nanomaterials have spawned a renewed interest in the field. Some inherent differences in the luminescent properties of these nanocrystalline particles compared to conventional single crystals (bulk) include changes in the emission lifetime, intensity, and emission resolution. In fact, these properties depend strongly on the size of the nanoparticles.[1,2]

Lanthanide-doped nanocrystals prove very interesting in that the trivalent dopant ions have many electronic energy levels, some of which are suitable for direct pumping by common laser sources. Additionally, many of these energy levels are quasi-evenly spaced such that multiple resonant excitation from an excited state can occur, and in turn leads to upconversion. This latter phenomenon is basically defined as the process involving the emission of photons whose energies are superior to those of the incident photons.[3] Moreover, the associated long lifetimes of these energy levels are such that they facilitate the upconversion process by leading to a significant buildup of the population in the intermediate excited state (population reservoir), which is essential if the mechanism is to proceed with reasonable efficiency. The process of upconversion in Ln^{3+}-doped inorganic materials has been investigated by a number of researchers in a variety of different hosts (see review 4, for example) from single crystals to glasses but to a much lesser extent in nanomaterials.[5−9]

The Tm^{3+} ion used as a dopant in inorganic nanocrystals has been shown to readily undergo red-to-blue upconversion.[10] However, the drawback with this scheme is that the pump laser required is expensive and rather cumbersome and thus does not constitute a very appealing means of obtaining blue (or UV) upconverted light. On the other hand, certain commercially available and relatively inexpensive sources of NIR emitting semiconductor diodes ($\lambda_{em} \approx 980$ nm) would offer a more cost-effective means for any application involving the upconversion from NIR to visible light. However, the Tm^{3+} ion has no energy level that can be efficiently and directly populated with 980 nm radiation, so to overcome this, another lanthanide ion, Yb^{3+}, can be used as a sensitizer. The benefit of codoping with Yb^{3+} is that it possesses only two energy levels, the $^2F_{7/2}$ ground state and the $^2F_{5/2}$ excited state. The latter has a high cross section of absorption and in turn leads to an increase in the upconversion efficiency compared with direct pumping. Following the excitation of the Yb^{3+} ion, multiple energy transfer processes may occur from Yb^{3+} to Tm^{3+} which makes upconversion to the blue and UV emitting excited states possible.[11]

The development of a nanomaterial that is capable of being excited in the near-infrared and emitting from the visible (and in some cases the UV) has potentially many applications. Some of the major ones include biological markers,[12] and consumer electronics for use as efficient 3D high-resolution display phosphors.[13] For some of these applications, the nanoparticles

* To whom correspondence should be addressed. Phone: 1-514-848-2424, ext 3350. Fax: 1-514-848-2868. E-mail: capo@vax2.concordia.ca.
[†] Concordia University.
[‡] Università di Verona.

10.1021/jp052192w CCC: $30.25
Published on Web 00/00/0000 PAGE EST: 5.4

must no doubt be dispersed in an appropriate solvent to satisfy the requirements of the device. Upconversion in colloidal solutions has been shown by Güdel et al. on lanthanide phosphate ($LuPO_4$:Tm^{3+}, Yb^{3+} and $YbPO_4$:Er^{3+}) and fluoride ($NaYF_4$:RE^{3+}, Yb^{3+}) nanoparticles.[14] However, the study of the upconversion in the dry material provides invaluable insight to the spectroscopic behavior of the upconverting material. In this paper, we present such a study on the upconversion properties of $Gd_3Ga_5O_{12}$ nanoparticles codoped with 1% both of Tm^{3+} and Yb^{3+}, and discuss the relevant mechanisms associated with the upconversion process.

2. Experimental Section

2.1. Sample Preparation. Gadolinium gallium garnet ($Gd_3Ga_5O_{12}$, GGG) nanocrystals codoped with 1% each of Tm^{3+} and Yb^{3+} ($Gd_{2.94}Tm_{0.03}Yb_{0.03}Ga_5O_{12}$) were prepared via a solution combustion (propellant) synthesis procedure.[15−17] An aqueous solution containing the appropriate molar ratios of carbohydrazide $(NH_2NH)_2CO$ (Aldrich, 98%), $Gd(NO_3)_3{\cdot}6H_2O$ (Aldrich, 99.99%), $Ga(NO_3)_3{\cdot}H_2O$ (Aldrich, 99.999%), $Tm(NO_3)_3{\cdot}6H_2O$ (Aldrich, 99.9%), and $Yb(NO_3)_3{\cdot}5H_2O$ (Aldrich, 99.9%) was prepared having an oxidant-to-reductant (carbohydrazide-to-metal nitrate) molar ratio of 2.5. This aqueous precursor solution was heated with a Bunsen flame to evaporate the water, after which the autocombustion process began with the evolution of a brown fume. After a very short time (within a few seconds), a remarkably porous voluminous mass of powder was formed. The proposed stoichiometric equation for the synthesis reaction is given below:

$$3(1-x-y)Gd(NO_3)_3 + 3xTm(NO_3)_3 + 3yYb(NO_3)_3 + 5Ga(NO_3)_3 + 3(NH_2NH)_2CO \rightarrow (Gd_{1-x-y}Tm_xYb_y)_3Ga_5O_{12} + 24NO_2 + 6N_2 + 3CO_2 + 9H_2O$$

where in this case $x = 0.01$ and $y = 0.01$.

Once the synthesis reaction has completed, any unreacted carbohydrazide and/or nitrate ions were decomposed by heating the synthesized powders at 500 °C for 1 h. The particles had an average diameter of approximately 20 nm, when analyzed by wide-angle powder X-ray diffraction.[18]

No other actions were taken to prevent the nanosample from coming into contact with the ambient atmosphere, as surface adsorbed components are not significant for the GGG samples.[17] The nanocrystalline powder was placed in a glass capillary for all spectroscopic investigations.

2.2. UV, Visible, and NIR Room-Temperature Emission Spectroscopy (λ_{exc} = 465.8 and 980 nm). The direct excitation visible emission spectra were obtained from a Coherent Sabre Innova, 20 W argon laser, using the 465.8 nm line as the excitation source. The upconverted emission spectra were obtained using 980 nm from a Spectra-Physics model 3900 Ti sapphire laser pumped by the 514.5 nm line of the Coherent Sabre Innova Ar^+ laser. UV emissions were recorded with a Spex Minimate 1/4 m monochromator and detected with an Oriel 70680 photomultiplier tube. Visible emissions were collected from the $Gd_3Ga_5O_{12}$:Tm^{3+}, Yb^{3+} nanocrystals at $\pi/2$ from the incident beam and then dispersed by a 1 m Jarrell-Ash Czerny-Turner double monochromator. The visible emissions from the sample exiting the monochromator were detected by a thermoelectrically cooled Hamamatsu R943-02 photomultiplier tube and the photomultiplied signals were processed by a Stanford Research Systems (SRS) model SR440 preamplifier. A Stanford Research Systems model SR 400 gated photon counter data acquisition system was used as an interface between the spectroscopic equipment and the computer running the SRS SR 465 data acquisition software. The near-infrared emission spectra were recorded using a Jarrell-Ash 3/4 m Czerny-Turner single monochromator in second order and the signal was detected with a liquid nitrogen cooled North Coast EO-817P germanium detector connected to a computer-controlled Stanford Research Systems SR 510 lock-in amplifier. Luminescent spectra obtained were not corrected for instrumental response.

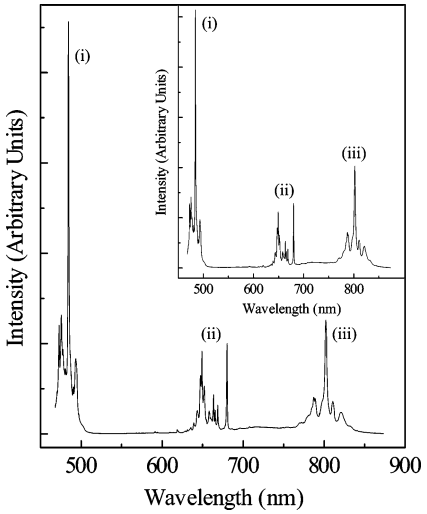

Figure 1. Room temperature visible emission spectrum (λ_{exc} = 465.8 nm) of nanocrystalline $Gd_3Ga_5O_{12}$:Tm^{3+}, Yb^{3+} and $Gd_3Ga_5O_{12}$:Tm^{3+} (inset) showing the (i) $^1G_4-{}^3H_6$, (ii) $^1G_4-{}^3F_4$, and (iii) $^3H_4-{}^3H_6$ transitions.

Decay curves for each manifold were obtained by modulation of the 465.8 and 980 nm excitation wavelengths through the use of a Stanford Research Systems SR 540 optical chopper. The emission from the sample was fed into the same data acquisition system as above.

All spectroscopic measurements were performed at room temperature.

3. Results and Discussion

3.1. Luminescence Spectroscopy. The room temperature emission spectrum (Figure 1) was obtained for nanocrystalline $Gd_3Ga_5O_{12}$:Tm^{3+}, Yb^{3+} using 465.8 nm as the excitation wavelength, which corresponds to excitation into the $^1G_4$ excited energy level of the Tm^{3+} ion. A dominant blue-green emission centered at approximately 485 nm was observed and assigned to the $^1G_4-{}^3H_6$ transition. Red emission between 640 and 680 nm was also seen, corresponding to the $^1G_4-{}^3F_4$ transition. Last, emission in the near-infrared was noted from about 760−840 nm, which is assigned to the $^1G_4-{}^3H_5/{}^3H_4-{}^3H_6$ transitions. Figure 1 (inset) shows the emission spectrum of singly doped GGG:Tm^{3+} (1%) nanocrystals. Clearly, the addition of Yb^{3+} does not affect the visible emission of this material.

Interestingly, the Yb^{3+} ion possesses only one excited state ($^2F_{5/2}$) centered at approximately 1000 nm. This is ideal from the point of view of upconversion where the $^2F_{5/2}$ state can act as the population reservoir in the upconversion process when pumping with 980 nm radiation. However, following excitation with 465.8 nm, it is conceivable that only emissions from the Tm^{3+} ion should be observed. Figure 2 presents a portion of the NIR emission spectrum of GGG:Tm^{3+}, Yb^{3+} following excitation with 465.8 nm and a strong emission is observed between 900 and 1120 nm. Since Tm^{3+} has no emission between

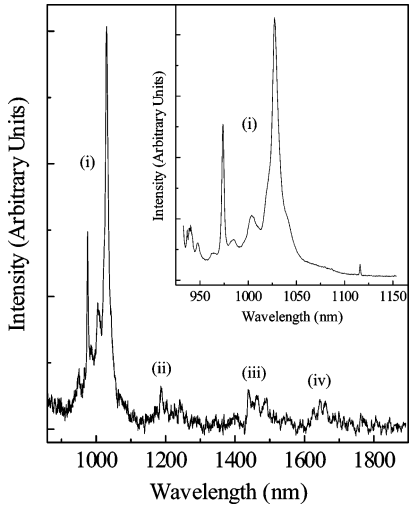

Figure 2. Room temperature NIR emission spectrum ($\lambda_{exc} = 465.8$ nm) showing the (i) $^2F_{5/2}-^2F_{7/2}$ (of Yb^{3+}), (ii) $^3H_5-^3H_6$, (iii) $^3H_4-^3F_4$, and (iv) $^3F_4-^3H_6$ transitions. Inset: Room temperature NIR emission spectrum ($\lambda_{exc} = 930$ nm) showing the (i) $^2F_{5/2}-^2F_{7/2}$ emission in $Gd_3Ga_5O_{12}:Yb^{3+}$ nanocrystals.

TABLE 1: Effective Decay Time Constants, τ_m, for Nanocrystalline $Gd_3Ga_5O_{12}:Tm^{3+}$ (1%) and $Gd_3Ga_5O_{12}:Tm^{3+}$, Yb^{3+} (1% each of Tm^{3+} and Yb^{3+}) Following excitation with 465.8 nm and $Gd_3Ga_5O_{12}:Tm^{3+}$, Yb^{3+} with 980 nm

	effective decay time constant, τ_m (μs)		
	$\lambda_{exc} = 465.8$ nm		$\lambda_{exc} = 980$ nm
transition	$Gd_3Ga_5O_{12}:Tm^{3+}$	$Gd_3Ga_5O_{12}:Tm^{3+}$, Yb^{3+}	$Gd_3Ga_5O_{12}:Tm^{3+}$, Yb^{3+}
$^1D_2-^3F_4$			312
$^1G_4-^3H_6$	425	418	536
$^1G_4-^3F_4$	442	426	554
$^1G_4-^3H_5/^3H_4-^3H_6$	641	546	552

900 and 1120 nm, the band in that region is ascribed to the Yb^{3+} $^2F_{5/2}-^2F_{7/2}$ emission, which undoubtedly occurs via a Tm^{3+} to Yb^{3+} energy transfer since there cannot be a direct population of the upper $^2F_{5/2}$ energy state of Yb^{3+} through the use of the 465.8 nm excitation wavelength. Furthermore, minor NIR emissions from the Tm^{3+} ion centered at 1200, 1450, and 1670 nm are observed and attributed to $^3H_5-^3H_6$, $^3H_4-^3F_4$, and $^3F_4-^3H_6$ transitions, respectively. Figure 2 (inset) presents the $^2F_{5/2}-^2F_{7/2}$ NIR emission of nanocrystalline GGG:Yb^{3+} (1%) following excitation with 930 nm.

Proof for this $Tm^{3+} \rightarrow Yb^{3+}$ energy transfer mechanism is found by comparing the decay times of GGG:Tm^{3+} (1%) and GGG:Tm^{3+}, Yb^{3+} (1% each of Tm^{3+} and Yb^{3+}) following 465.8 nm excitation. The decay curves for GGG:Tm^{3+} and GGG:Tm^{3+}, Yb^{3+} nanocrystalline samples deviated from exponentiality and thus were fit with the equation proposed by Nakazawa:[19]

$$\tau_m = \frac{\int_0^\infty tI(t)\,dt}{\int_0^\infty I(t)\,dt} \quad (1)$$

where τ_m is the effective decay time constant, and $I(t)$ is the intensity at time t. Thus, using this method, the effective decay time constants, τ_m, were obtained (Table 1). We observe that the effective decay time constants of the $^1G_4$ emissions (for the $^1G_4 \rightarrow {}^3H_6$ and $^1G_4 \rightarrow {}^3F_4$ transitions) were not affected by the insertion of Yb^{3+}. In the absence of Yb^{3+} (GGG:Tm^{3+}, 1%), the lifetime of the $^1G_4$ state was determined to be 430 μs while in the presence of Yb^{3+}, the effective lifetime of the $^1G_4$ state was approximately 420 μs. In contrast, there is a significant change in the decay time constant of the manifold between 760 and 840 nm when codoping with 1% Yb^{3+} and it decreases from 641 μs in GGG:Tm^{3+} to 546 μs in GGG:Tm^{3+}, Yb^{3+} nanocrystals, a 100 μs decrease. This clearly indicates that the Tm^{3+} to Yb^{3+} energy transfer occurs from this state. Additionally, the lifetime of the Yb^{3+} $^2F_{5/2}$ state was measured following Tm^{3+} excitation ($\lambda_{exc} = 465.8$ nm) and an effective lifetime of 900 μs was determined.

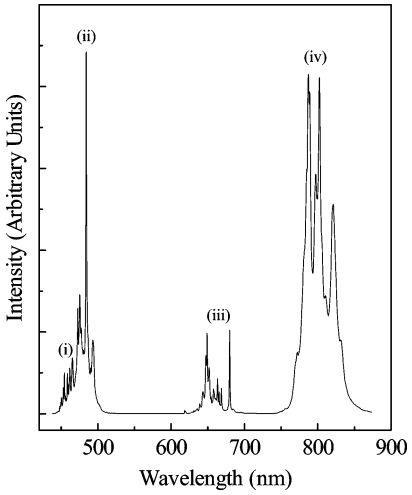

Figure 3. Room temperature upconversion spectrum ($\lambda_{exc} = 980$ nm) of nanocrystalline $Gd_3Ga_5O_{12}:Tm^{3+}$, Yb^{3+} showing the (i) $^1D_2-^3F_4$, (ii) $^1G_4-^3H_6$, (iii) $^1G_4-^3F_4$, and (iv) $^1G_4-^3H_5/^3H_4-^3H_6$ visible transitions.

Conversely, the lifetime of the Yb^{3+} $^2F_{5/2}$ excited state changes considerably in the presence (and absence) of Tm^{3+}. In the absence of energy transfer (no Tm^{3+} codoping), the lifetime ($\lambda_{exc} = 930$ nm) of the $^2F_{5/2}$ state in GGG:Yb^{3+} was determined to be 1180 μs. However, when 1% Tm^{3+} was added to the matrix, a lifetime of 500 μs was obtained for the $^2F_{5/2}$ Yb^{3+} state of GGG:Tm^{3+}, Yb^{3+} nanocrystals. We can calculate the efficiency of the $Yb^{3+} \rightarrow Tm^{3+}$ energy transfer (η_τ) from[20]

$$\eta_\tau = 1 - \frac{\tau_{DA}}{\tau_D} \quad (2)$$

where τ_{DA} (500 μs) is the lifetime of the donor (D, Yb^{3+}) in the presence of the acceptor (A, Tm^{3+}) and τ_D (1180 μs) is the lifetime of the donor in the absence of the acceptor. Thus, the efficiency of the energy transfer was determined to be 0.576.

3.2. Upconversion Luminescence Spectroscopy. Excitation with 500 mW (800 W/cm^2) of 980 nm light to directly populate the $^2F_{5/2}$ energy level of Yb^{3+} subsequently leads to an energy transfer to the $^3H_5$ energy level of Tm^{3+} of the following type: $^2F_{5/2}$ (Yb^{3+}), $^3H_6$ (Tm^{3+}) $\rightarrow$ $^2F_{7/2}$ (Yb^{3+}), $^3H_5$ (Tm^{3+}). Following this, a series of upconversion processes can occur, each with their own end result, and these will be discussed in further detail later on.

Resulting from the irradiation of the sample with 980 nm, upconverted emission in the UV, blue, blue-green, red, and near-infrared was observed (Figures 3 and 4). Ultraviolet upconverted emission was observed in the region of 360−380 nm and ascribed to the $^1D_2-^3H_6$ transition. Blue emission was observed centered at ca. 454 nm and assigned to the energy transition $^1D_2-^3F_4$. A much more intense blue-green emission resulting from the $^1G_4-^3H_6$ transition was observed centered at 484 nm and red upconverted emission resulting from the $^1G_4-^3F_4$

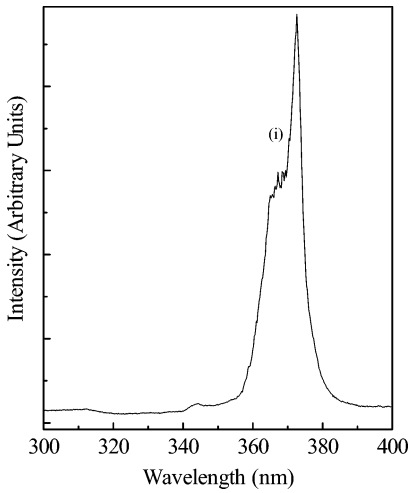

Figure 4. Room temperature upconversion spectrum ($\lambda_{exc} = 980$ nm) of nanocrystalline $Gd_3Ga_5O_{12}$:Tm^{3+}, Yb^{3+} showing the (i) $^1D_2-{}^3H_6$ UV transition.

TABLE 2: Number of Photons (*n*) Involved in the Upconversion Mechanism(s) Determined Experimentally for Nanocrystalline $Gd_3Ga_5O_{12}$:Tm^{3+}, Yb^{3+} Following Excitation with 980 nm

	no. of photons (*n*)	
transition	expected	obsd
$^1D_2-{}^3F_4$	4	2.99
$^1G_4-{}^3H_6$	3	2.05
$^1G_4-{}^3F_4$	3	2.09
$^1G_4-{}^3H_5/{}^3H_4-{}^3H_6$	2	1.47

transition was noted between 640 and 680 nm. Finally, intense NIR emission was observed between 760 and 840 nm corresponding to the $^1G_4-{}^3H_5/{}^3H_4-{}^3H_6$ transitions. It should be noted that cooperative upconversion involving Yb^{3+} pairs was not observed in the GGG:Tm^{3+}, Yb^{3+} nanocrystals studied. Moreover, studies on singly doped nanocrystalline GGG:Yb^{3+} have shown that at this particle size (20 nm) and up to a 10 mol % doping level, no cooperative upconversion was observed.

To better understand the mechanism(s) by which the upper emitting states are populated, we investigated the dependence of the upconverted emission intensity on the pump power. For an unsaturated upconversion process, it is possible to determine the number of photons (*n*) required to populate the emitting state from the slope of the graph of ln(intensity) versus ln(power) according to

$$I \propto P^n \tag{3}$$

where the upconverted luminescence intensity (*I*) is proportional to the *n*th power of the low-frequency excitation power (*P*).[21,22] The summary of the power study is given in Table 2. The above relation holds for low excitation powers only and under high excitation densities, the upconversion processes will saturate. Upconversion is a nonlinear process and as a consequence of the conservation of energy, it cannot maintain its nonlinear behavior up to infinite excitation. Therefore, the power dependence does not follow the above straightforward relation at higher pump powers. Thus, we obtain slopes (*n*) which deviate from the expected values in cases where the influence of upconversion is large (i.e., high pump densities).[22]

The effective decay time constants were obtained for the $^1D_2$, $^1G_4$, and $^3H_4$ emitting states following excitation with 980 nm and were compared to the decay times obtained when directly populating the upper emitting states ($\lambda_{exc} = 465.8$ nm) (Table 1). As can be seen in Table 1, the decay time constants of the $^1G_4$ and $^3H_4$ excited states are lengthened when comparing upconversion ($\lambda_{exc} = 980$ nm) to emission ($\lambda_{exc} = 465.8$ nm) phenomena. This is consistent with the idea of an ETU mechanism, which is one of the mechanisms proposed for the population of the excited Tm^{3+} energy levels through successive energy transfers from excited Yb^{3+} ions. On the other hand, if one examines the data in Table 1 in more detail, it seems that the observed decay times for the $^1G_4-{}^3H_6$, $^1G_4-{}^3F_4$, and $^1G_4-{}^3H_5/{}^3H_4-{}^3H_6$ transitions are all similar, which may possibly be explained by the fact that it is the lifetime of the feeding state ($^2F_{5/2}$ of Yb^{3+}) being measured and since all excitations must proceed by ETU, this would be the bottleneck for the upconversion processes. The lifetime of the Yb^{3+} emission ($\lambda_{exc} = 930$ nm) in the presence of energy transfer was determined to be 500 μs.

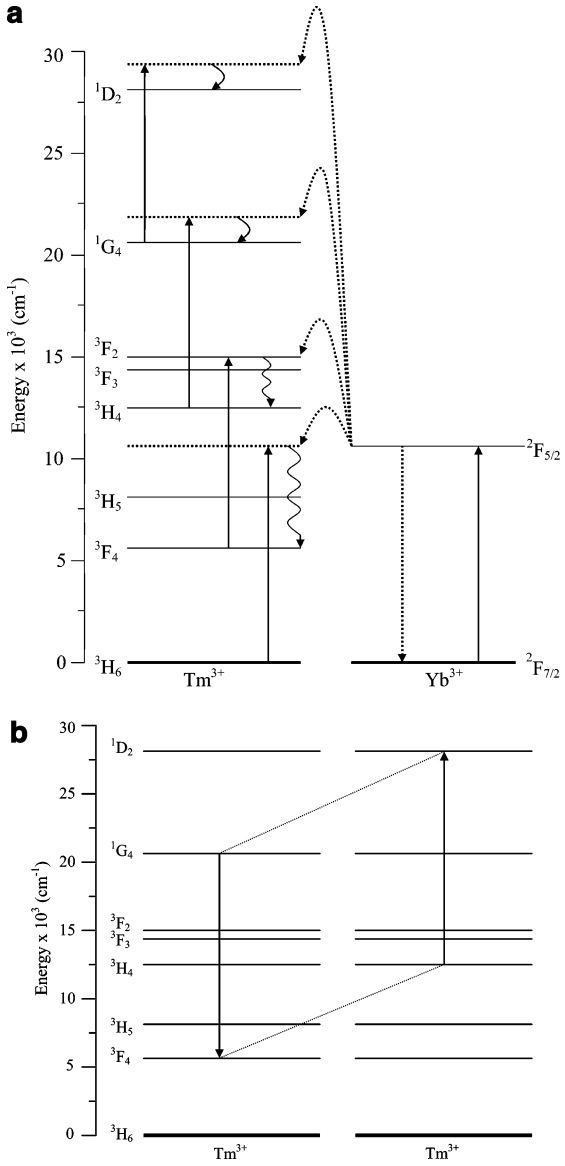

Figure 5. (a) The energy levels diagrams of the Tm^{3+} and Yb^{3+} dopant ions and possible upconversion processes following excitation with 980 nm. (b) Schematic representation of the Tm^{3+} ($^1G_4$, $^3H_4$) → ($^3F_4$, $^1D_2$) ion pair process responsible for populating the $^1D_2$ state.

A schematic representation of the Yb^{3+} to Tm^{3+} upconversion processes is depicted in Figure 5a. Following the initial absorption of the 980 nm pump photon, the Yb^{3+} ion is excited from the $^2F_{7/2}$ ground state to the $^2F_{5/2}$ excited state (ground-

state absorption). The excited Yb^{3+} ion transfers its energy nonresonantly to the Tm^{3+} ion exciting it from the $^3H_6$ ground state to the $^3H_5$ excited state[11] where the excess energy (approximately 1600 cm^{-1}) can be dissipated by the host lattice (the highest phonon energy of the GGG nanocrystal lattice is approximately 600 cm^{-1}). Multiphonon relaxation in turn populates the $^3F_4$ state. The Tm^{3+} ion is subsequently resonantly excited to the $^3F_2$ state via a second transfer of energy from the excited Yb^{3+} ion to the Tm^{3+} ion in the $^3F_4$ intermediate state. Alternately, the $^3F_2$ state may be populated via resonant excited-state absorption (ESA) of the $^3F_4$ state to the $^3F_2$ state. This process would be more efficient since it is independent of the $Tm^{3+}-Yb^{3+}$ distance and coupling. Thus, following population of the $^3F_2$ level, the thulium ion in turn relaxes nonradiatively via multiphonon relaxation to the $^3H_4$ state after which the $^3H_4-{}^3H_6$ radiative emission occurs. Upon comparison of the direct emission ($\lambda_{exc} = 465.8$ nm) and upconversion ($\lambda_{exc} = 980$ nm) spectra, it is clear that there is a severe change in the relative emission intensity of the NIR transition between 760 and 840 nm compared to the intensity of the other manifolds within the spectrum. This change in the relative intensity is a direct result of the proposed upconversion mechanism. As stated earlier, the NIR emission centered at approximately 800 nm is due to the overlapping $^1G_4-{}^3H_5$ and $^3H_4-{}^3H_6$ transitions.[23] When irradiating the nanocrystals with 465.8 nm, the $^1G_4$ state is excited directly. The energy gap between the $^1G_4$ and the next lower lying state, $^3F_2$, is approximately 5900 cm^{-1}. The observed rate of depopulation W_{obs} of an excited state could be expressed as the sum of the radiative, W_R, and multiphonon transition probabilities, W_{MPR}. In fact, the rate of multiphonon relaxation is dominated by[24]

$$(1 + n_{eff})^p \tag{4}$$

where

$$n_{eff} = [\exp(\hbar\omega_{eff}/kT) - 1]^{-1} \tag{5}$$

is the occupancy of the effective phonon mode of energy ($\hbar\omega_{eff}$) and p is the number of phonons necessary to bridge the energy gap between the emitting level and the next lower level. Thus, it would require approximately 10 GGG phonons to bridge the energy gap between the $^1G_4$ and $^3F_2$ states. The result is that the $^1G_4$ state will be depopulated either radiatively through the emission of photons or via a cross-relaxation process. As a result, since the $^3H_4$ state is populated mostly via multiphonon relaxation from the upper states, it is clear that the population of this state will be low and, consequently, the emission intensity of the $^3H_4-{}^3H_6$ will be low. On the other hand, when pumping with 980 nm, two successive transfers of energy from Yb^{3+} will populate the $^3F_2$ state directly. The Tm^{3+} ion will immediately decay to the $^3F_3$ state as the energy gap is only ~640 cm^{-1} and requires only one GGG phonon. The energy gap between the $^3F_3$ state and the $^3H_4$ state is on the order of 1800 cm^{-1}. Therefore, the probability that the $^3H_4$ state is populated via nonradiative decay from this state is very high as it only requires 3 GGG phonons. This would obviously lead to higher emission intensity in the upconversion spectrum compared to the spectrum obtained when utilizing 465.8 nm to directly excite the $^1G_4$ state.

Following this initial process, another excited Yb^{3+} ion in close proximity can also transfer its energy nonresonantly to the Tm^{3+} ion in the $^3H_4$ intermediate state, thus exciting the ion to the $^1G_4$ state (third energy transfer). Again, the excess energy (approximately 1800 cm^{-1}) is dissipated by the $Gd_3Ga_5O_{12}$ lattice vibrations. This in turn leads to the $^1G_4-{}^3F_4$ (red) and $^1G_4-{}^3H_6$ (blue-green) transitions. Finally, it is possible that the Tm^{3+} ion is excited to the $^1D_2$ state via a fourth nonresonant transfer of energy from a Yb^{3+} ion to a Tm^{3+} ion in the $^1G_4$ level. The population of the $^1D_2$ state can lead to the radiative emission of a UV photon via the $^1D_2-{}^3H_6$ transition or a blue photon via the $^1D_2-{}^3F_4$ transition. It should be noted that there is an alternate possibility for the promotion of a Tm^{3+} ion into the $^1D_2$ energy level. There exists a resonant mechanism involving an excited Tm^{3+} ion in the $^1G_4$ level and another in the $^3H_4$ level (Figure 5, inset). One Tm^{3+} ion in the $^3H_4$ state will interact with another Tm^{3+} ion in the $^1G_4$ state undergoing an ion-pair process of the type ($^1G_4$, $^3H_4$) → ($^3F_4$, $^1D_2$), which populates the $^1D_2$ level. However, since the ($^1G_4$, $^3H_4$) → ($^3F_4$, $^1D_2$) ion-pair process depopulates the $^3H_4$ state, it is clear that the influence of this mechanism is small given the relatively high intensity of the $^3H_4-{}^3H_6$ transition. Last, it is rather interesting to note that in Y_2O_3:Tm^{3+}, Yb^{3+} single crystals, no emission from excited states higher than $^1G_4$ was observed.[23]

Experiments are currently well underway to help better understand the NIR-to-blue (and UV) upconversion in $Gd_3Ga_5O_{12}$:Tm^{3+}, Yb^{3+} nanocrystals. We are in the process of examining both the effects of temperature and Yb^{3+} concentration on the upconversion properties as well as utilizing pulsed NIR excitation to study the upconversion kinetics. These will be the subject of a future paper.

4. Conclusions

The goal of these experiments was to study a nanocrystalline sample capable of undergoing efficient upconversion into the visible and UV when being excited with NIR radiation. The GGG:Tm^{3+}, Yb^{3+} sample studied is capable of this upconversion process and for this reason can possibly be used in such applications as was previously noted: biological markers and consumer applications such as efficient and high-resolution display phosphors.

A spectroscopic analysis of the luminescence from GGG:Tm^{3+}, Yb^{3+} nanocrystals (1% each of Tm^{3+} and Yb^{3+}) was undertaken. Excitation of the Tm^{3+} $^1G_4$ excited state with 465.8 nm radiation showed blue-green, red, and NIR emissions from the $^1G_4-{}^3H_6$, $^1G_4-{}^3F_4$, and $^1G_4-{}^3H_5/{}^3H_4-{}^3H_6$ transitions, respectively. Examination of the NIR emission spectrum showed the presence of the $^2F_{5/2}-{}^2F_{7/2}$ Yb^{3+} transition indicating that a Tm^{3+} to Yb^{3+} energy transfer was present. Upon comparison of the decay time constants for nanocrystalline singly doped GGG:Tm^{3+} (1%) and the GGG:Tm^{3+}, Yb^{3+} sample under investigation, it was determined that the energy transfer occurred via the $^3H_4$ state of Tm^{3+}.

Following excitation of the $^2F_{5/2}$ state of Yb^{3+}, intense upconversion was observed in the UV, blue, blue-green, red, and NIR regions of the spectrum. The upconversion occurred via successive resonant and nonresonant energy transfers from the Yb^{3+} ion to the Tm^{3+} ion since the Tm^{3+} ion has no energy level, which can be directly pumped with 980 nm. The upconversion spectrum showed an increase in the relative emission intensity of the NIR transition centered at 800 nm compared to the direct excitation spectrum obtained using 465.8 nm. This was the result of an increase in the intensity of the $^3H_4-{}^3H_6$ emission following efficient multiphonon relaxation from the $^3F_2$ state to the $^3F_3$ state.

The power dependence studies showed a deviation for n, the expected number of photons partaking in the upconversion process, indicating a saturation of this process at high pumping intensities. The efficiency of the Yb^{3+} to Tm^{3+} energy transfer

was determined from the effective decay times of Yb^{3+} in the presence and absence of energy transfer. The energy transfer efficiency, η, was determined to be 0.576.

Acknowledgment. The authors gratefully thank Erica Viviani (Università di Verona, Italy) for expert technical assistance. The authors acknowledge the Natural Science and Engineering Research Council of Canada and MIUR of Italy (Project 2003035190_001), for financial support.

References and Notes

(1) Sharma, P. K.; Nass, R.; Schmidt, H. *Opt. Mater.* **1998**, *10*, 161−169.
(2) Williams, D. K.; Yuan, H.; Tissue, B. M. *J. Lumin.* **1999**, *83*−*84*, 297−300.
(3) Scheps, R. *Prog. Quantum Electron.* **1996**, *20*, 271−358.
(4) Auzel, F. *Chem. Rev.* **2004**, *104*, 139−173.
(5) Hirai, T.; Orikoshi, T.; Komasawa, I. *Chem. Mater.* **2002**, *14*, 3576−3583.
(6) Matsuura, D. *Appl. Phys. Lett.* **2002**, *81*, 4526−4528.
(7) Silver, J.; Martinez-Rubio, M. I.; Ireland, T. G.; Fern, G. R.; Withnall, R. *J. Phys. Chem. B* **2001**, *105*, 948−953.
(8) Yi, G.; Sun, B.; Yang, F.; Chen, D.; Zhou, Y.; Cheng, J. *Chem. Mater.* **2002**, *14*, 2910−2914.
(9) Zhang, H. X.; Kam, C. H.; Zhou, Y.; Han, H. Q.; Buddhudu, S.; Lam, Y. L. *Opt. Mater.* **2000**, *15*, 47−50.
(10) Vetrone, F.; Boyer, J. C.; Capobianco, J. A.; Speghini, A.; Bettinelli, M. *Nanotechnology* **2004**, *15*, 75−81.
(11) Ostermayer, F. W.; van der Ziel, J. P.; Marcos, H. M.; Van Uitert, L. G.; Geusic, J. E. *Phys. Rev. B* **1971**, *3*, 2698−2705.
(12) Niedbala, R. S.; Feindt, H.; Kardos, K.; Vail, T.; Burton, J.; Bielska, B.; Li, S.; Milunic, D.; Bourdelle, P.; Vallejo, R. *Anal. Biochem.* **2001**, *293*, 22−30.
(13) Downing, E.; Hesselink, L.; Ralston, J.; Macfarlane, R. *Science* **1996**, *273*, 1185−1189.
(14) Heer, S.; Lehmann, O.; Haase, M.; Güdel, H. U. *Angew. Chem., Int. Ed.* **2003**, *42*, 3179−3182.
(15) Tao, Y.; Zhao, G.; Zhang, W.; Xia, S. *Mater. Res. Bull.* **1997**, *32*, 501−506.
(16) Tessari, G.; Bettinelli, M.; Speghini, A.; Ajò, D.; Pozza, G.; Depero, L. E.; Allieri, B.; Sangaletti, L. *Appl. Surf. Sci.* **1999**, *144*−*145*, 686−689.
(17) Vetrone, F.; Boyer, J. C.; Capobianco, J. A.; Speghini, A.; Bettinelli, M. *J. Phys. Chem. B* **2003**, *107*, 10747−10752.
(18) Krsmanovic, R.; Polizzi, S.; Canton, P. *Mater. Sci. Forum* **2005**, *494*, 143−148.
(19) Nakazawa, E. In *Phosphor Handbook*; Shionoya, S., Yen, W. M., Eds.; CRC Press: Boca Raton, FL, 1999; p 102.
(20) de Sousa, D. F.; Batalioto, F.; Bell, M. J. V.; Oliveira, S. L.; Nunes, L. A. O. *J. Appl. Phys.* **2001**, *90*, 3308−3313.
(21) Chamarro, M. A.; Cases, R. *J. Lumin.* **1988**, *42*, 267−274.
(22) Pollnau, M.; Gamelin, D. R.; Lüthi, S. R.; Güdel, H. U.; Hehlen, M. P. *Phys. Rev. B* **2000**, *61*, 3337−3346.
(23) Guyot, Y.; Moncorgé, R.; Merkle, L. D.; Pinto, A.; McIntosh, B.; Verdun, H. *Opt. Mater.* **1996**, *5*, 127−136.
(24) Riseberg, L. A.; Moos, H. W. *Phys. Rev.* **1968**, *174*, 429−438.